Letter | Editors' Suggestion

Tunable topological magnetism in superlattices of nonmagnetic B20 systems

Vladislav Borisov [1,*], Anna Delin [2,3,4] and Olle Eriksson [1,5]

[1]*Department of Physics and Astronomy, Uppsala University, Box 516, SE-75120 Uppsala, Sweden*

[2]*Department of Applied Physics, School of Engineering Sciences, KTH Royal Institute of Technology, AlbaNova University Center, SE-10691 Stockholm, Sweden*

[3]*Wallenberg Initiative Materials Science for Sustainability (WISE), KTH Royal Institute of Technology, SE-10044 Stockholm, Sweden*

[4]*SeRC (Swedish e-Science Research Center), KTH Royal Institute of Technology, SE-10044 Stockholm, Sweden*

[5]*Wallenberg Initiative Materials Science for Sustainability, Uppsala University, SE-75121 Uppsala, Sweden*

(Received 27 September 2023; revised 27 April 2024; accepted 19 July 2024; published 8 August 2024)

We predict topological magnetic properties of B20 systems, that are organized in atomically thin multilayers. In particular, we focus on FeSi/CoSi and FeSi/FeGe superlattices with different numbers of layers and interface structures. We demonstrate that the absence of long-range magnetic order, previously observed in bulk FeSi and CoSi, is broken near the FeSi/CoSi interface, where a magnetic state with a nontrivial topological texture appears. Using the Heisenberg and Dzyaloshinskii-Moriya (DM) interactions calculated from first principles, we perform finite-temperature atomistic spin dynamics simulations for up to 2×10^6 spins to capture the complexity of noncollinear textures. Our simulations predict the formation of antiskyrmions in a [001]-oriented FeSi/CoSi multilayer, intermediate skyrmions in a [111]-oriented FeSi/CoSi system, and Bloch skyrmions in the FeSi/FeGe (001) system, with a size between 7 and 37 nm. These varieties of topological magnetic textures in the studied systems can be attributed to the complex asymmetric structure of the DM matrix, which is different from previously known magnetic materials. We demonstrate that through structural engineering both ferromagnetic and antiferromagnetic skyrmions can be stabilized, where the latter are especially appealing for applications due to the zero skyrmion Hall effect. The proposed B20 multilayers show a potential for further exploration and call for experimental confirmation.

DOI: 10.1103/PhysRevB.110.L060407

Introduction. A large part of information is nowadays stored magnetically in hard disk drives where oppositely polarized ferromagnetic domains encode the "1" and "0" bits. While this simple idea has significantly shaped the computer technology during the last decades, it has almost reached its limit in terms of information density and data access time [1]. New ways of magnetic information storage were suggested in 2013 [2] and later on extended in Ref. [3] where the idea is to use nanoscale topological magnetic objects [skyrmions, Figs. 1(a) and 1(b)] formed by winding atomic spins in a racetrack to store and process information. Topological magnetic textures can be used not just for storage but also for new types of computing (neuromorphic [4,5] and stochastic [6]). Understandably, searching for new systems hosting topological magnetic textures is an ongoing active effort in the research community (for a review, see Ref. [7]).

The B20 compound MnSi was the first observed bulk, solid state system with magnetic skyrmions [8]. Due to its cubic but noncentrosymmetric crystal structure, MnSi shows the Dzyaloshinskii-Moriya interaction (DMI) of well-known bulk type which corresponds to the micromagnetic energy density

$$\varepsilon_{\text{bulk}} = D\,\vec{m} \cdot (\vec{\nabla} \times \vec{m}), \tag{1}$$

where $\vec{m} = \vec{m}(\vec{r})$ is a continuous function describing the magnetization in different points of space and D is the strength of the DMI. It is only due to this kind of DMI that Bloch-type skyrmions, where spins rotate perpendicular to the radial direction [Fig. 1(a)], are stabilized in MnSi. This skyrmion type is observed in most bulk magnets with topological magnetic textures, except for lacunar spinels [9,10].

Skyrmions have also been found in transition metal multilayers, e.g., Ir/Fe/Co/Pt [11], Fe/Ir(111) [12], and Pd/Fe/Ir(111) [13], where the crystal symmetry is quite different. In many cases, these multilayers have a C_{3v} symmetry which leads to the so-called interfacial DMI [for details, see Ref. [14], Eq. (8)] described by the interfacial micromagnetic energy density

$$\varepsilon_{\text{int}} = D\left[m_x \frac{\partial m_z}{\partial x} - m_z \frac{\partial m_x}{\partial x} + m_y \frac{\partial m_z}{\partial y} - m_z \frac{\partial m_y}{\partial y}\right]. \tag{2}$$

This interaction, when sufficiently strong, stabilizes Néel skyrmions where spins rotate along the radial direction [Fig. 1(b)]. One can notice that the compounds building these nanoscale multilayers have no DMI in the bulk, and nonzero

*Contact author: vladislav.borisov@physics.uu.se

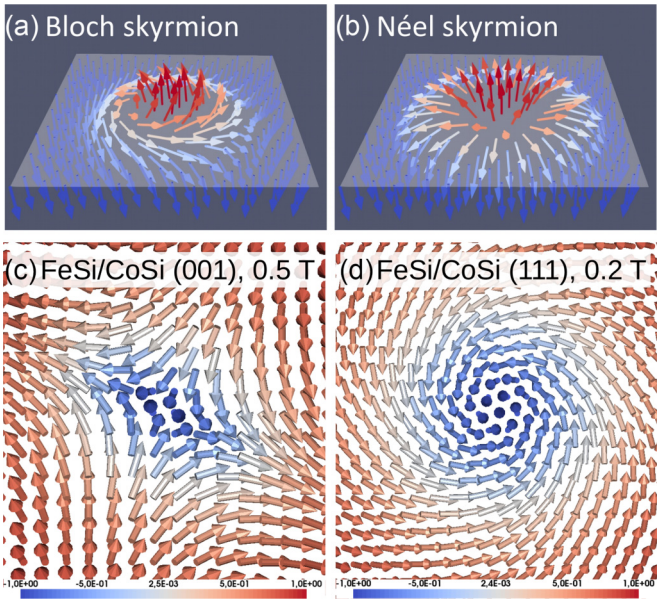

FIG. 1. Schematic spin configurations of (a) Bloch and (b) Néel skyrmions usually found in topological magnets. Examples of textures that we predict for B20 FeSi/CoSi multilayers based on atomistic spin dynamics in applied magnetic field: (c) antiskyrmion ($d = 7$ nm) and (d) intermediate skyrmion ($d = 12$ nm). The color code shows the z component of the magnetization.

DMI is induced by atomically sharp interfaces. Other interface symmetries (e.g., C_4) compatible with skyrmions have been analyzed as well for oxides [15] and Mn/W(001)-based multilayers [16].

The materials science community with a focus on systems with nontrivial magnetic topology has the ambition to find suitable materials with optimal size and stability of skyrmions to allow for technological applications. Theoretical calculations based on density functional theory offer a fast and rather reliable route to achieve this goal, although most successful predictions have been for magnetic materials where topology is not considered important. A notable example here is the tunneling magnetoresistance (TMR) effect that was predicted [17] before it was confirmed experimentally [18]. Other examples can be found in thin films and surfaces, where predictions of the enhancement of both spin- and orbital magnetic moments [19,20] preceded experiments [21,22]. Interestingly, new magnetic materials may be formed by a combination of elements that are nonmagnetic; $ZrZn_2$ and UGe_2 are perhaps the most well-known examples of this and, furthermore, they also exhibit ferromagnetism in combination with superconductivity [23].

The analysis above leads to the main idea of this Letter, which is to consider skyrmion magnetism in materials that are not even magnetic as bulk, but where the consideration of multilayers may induce magnetism and even topological magnetism. Examples of materials relevant here are pure FeSi [24] and CoSi [25]. Neither compound shows long-range magnetic order. However, magnetism is found in the alloy $Fe_{1-x}Co_xSi$, something which is due to a Stoner instability induced by the change of the electron count combined with peaks in the density of states.

The first example that we consider is the FeSi/CoSi multilayer. Based on crystal symmetry considerations, its constituents have a potential to host DMI in the bulk phase, at least when they are alloyed with each other to form the magnetic bulk $Fe_{1-x}Co_xSi$ compound, which is known to host Bloch skyrmions [26] and has a bulk-type DMI. For comparison, we also investigate another system, the FeSi/FeGe multilayer, where FeGe already has significant magnetic moments and nonzero DMI in the bulk. The underlying hypothesis of our work is that the interfaces in B20 multilayers can induce magnetism in the FeSi/CoSi system and overall a more complex DMI compared to the bulk B20 systems, and that this DMI will be tunable in a wide range in terms of magnitude and character, for example, by the thickness of the multilayer and interface structure.

It is necessary to note that thin films of FeGe were considered in the literature [27] and a huge enhancement of skyrmionic stability has been found when the film thickness is below the skyrmion lattice spacing ∼70 nm. However, for the thicknesses 15–75 nm considered in Ref. [27], the atomistic interface effects do not yet play any role. In our theoretical work, we focus on the FeSi/CoSi and FeSi/FeGe multilayers, which have not yet been studied experimentally and where the interface phenomena are important, with a goal to propose new topological magnetic systems.

Methods. To address the complex magnetic behavior of B20 multilayers that we propose in this Letter, we use a multiscale approach which describes the system step by step on increasing length scales (detailed accounts can be found in our recent works [28,29]). The first step is the calculation of the electronic properties using density functional theory [30] and the generalized gradient approximation in Perdew-Burke-Ernzerhof (GGA-PBE) parametrization [31] [a comparison with the local-spin-density approximation (LSDA) is considered in the Supplemental Material (SM) [32]; see also Refs. [33–38] therein], available in the full-potential linear muffin-tin orbital RSPT software [39–41]. We have verified that LSDA and GGA approximations predict similar magnetic moments (see discussion in Sec. VII in the SM [32]). For bulk $Fe_{1-x}Co_xSi$ we have also checked that the LSDA plus dynamical mean-field theory (LSDA + DMFT) approach (FLEX approximation) basically does not change the moments compared to LSDA. The FeSi/CoSi multilayer is modeled by a supercell with n unit cells of CoSi in the z direction and m unit cells of FeSi attached to CoSi. Periodic boundary conditions along the x, y, and z directions are imposed, meaning that the chosen model represents a superlattice with a repeated $(FeSi)_m/(CoSi)_n$ block. For brevity, we will also refer to this kind of structures as m/n superlattices.

We consider two different interface orientations, [001] and [111]. The former is constructed directly by stacking the bulk unit cells along one of the cubic lattice vectors, while the [111] structure is obtained using the atomic simulation environment [42,43]. In all cases, the crystal structure is fully optimized using the VASP code [44]. The same procedure is applied for the [001]-FeSi/FeGe multilayers. It is worth noting that the literature values of the lattice parameters of the corresponding bulk compounds are 4.485 Å (FeSi), 4.45 Å (CoSi), and 4.70 Å (FeGe). This means that the FeSi/CoSi multilayers are relatively weakly strained due to a small lattice mismatch of

0.8% between FeSi and CoSi. The FeSi/FeGe superlattices show a larger lattice mismatch of 4.8%.

To evaluate the changes of magnetic interactions between the Fe and Co moments near the interfaces compared to the bulk case, we calculated the Heisenberg and DM magnetic interactions using the Liechtenstein-Katsnelson-Antropov-Gubanov (LKAG) approach [45] (review in Ref. [46]), available in the RSPT software [39,40]. The system is then mapped onto an effective spin Hamiltonian,

$$H = -\sum_{j\neq i} J_{ij}(\vec{S}_i \cdot \vec{S}_j) - \sum_{j\neq i} \vec{D}_{ij} \cdot (\vec{S}_i \times \vec{S}_j), \qquad (3)$$

which contains several hundred interaction parameters J_{ij} and $\vec{D}_{ij}$ between different spin neighbors. With this information, we simulate the magnetic properties of the B20 multilayers at finite temperature and applied magnetic field using atomistic spin dynamics (ASD) and Monte Carlo simulations, available in the UPPASD code [47,48]. The ASD simulations are based on the Landau-Lifshitz-Gilbert equation [49,50],

$$\frac{\partial \vec{m}_i}{\partial t} = -\frac{\gamma}{1+\alpha^2}\left[\vec{m}_i \times \vec{B}_i + \frac{\alpha}{m}\vec{m}_i \times (\vec{m}_i \times \vec{B}_i)\right], \qquad (4)$$

which describes the time evolution of the magnetization $\vec{m}_i$ of a given spin i under the influence of the effective field $\vec{B}_i$. The latter is determined from the spin model [Eq. (3)] where, to a first approximation, we assume a zero on-site anisotropy. As is usual for Langevin dynamics, a random field proportional to $\sqrt{\alpha T}$ was added to $\vec{B}_i$ to simulate finite-temperature fluctuations, and the damping constant α is set to 1.0 to enable a fast convergence to the (quasi) equilibrium state. We perform these ASD simulations for a $(500 \times 500 \times 1)$ supercell with periodic boundary conditions, which contains 10^6 spins for the $(FeSi)_3/(CoSi)_3$ and 2×10^6 spins for the $(FeSi)_4/(CoSi)_1$ superlattice. The supercell cross sections correspond to a simulated region of around (220×220) nm^2 which allows to accommodate spin spiral and skyrmion phases.

While in the main text we focus on results obtained using spin model (3) where the character of DMI is important and is in the focus of the discussion, we also discuss the effect of moderate magnetocrystalline anisotropy that we calculate for the B20 multilayers on the magnetic textures in Sec. VIII of the SM [32].

$(FeSi)_m/(CoSi)_n$ superlattices. For these systems, we find the formation of finite magnetic moments on Fe and Co within a few atomic layers near the interfaces due to a changed electron count and Stoner instability, similarly to the bulk $Fe_{1-x}Co_xSi$ alloy. Further away from the interfaces, both FeSi and CoSi show no intrinsic magnetic moments, which is consistent with the magnetism for the bulk counterparts. This is illustrated in Fig. 2 on the example of the 3/3 superlattice where the induced moments are below 0.6 μ_B and localized around each FeSi/CoSi interface. Even for the 2/2 superlattice with a smaller thickness of FeSi and CoSi we find that the middle parts of the slabs are basically nonmagnetic and the overall profile of magnetization near the interfaces is very similar to that of the 3/3 superlattice (data not shown). However, for the 4/1 superlattice, where the CoSi layer is just 1 unit cell thick, we find that the whole CoSi becomes

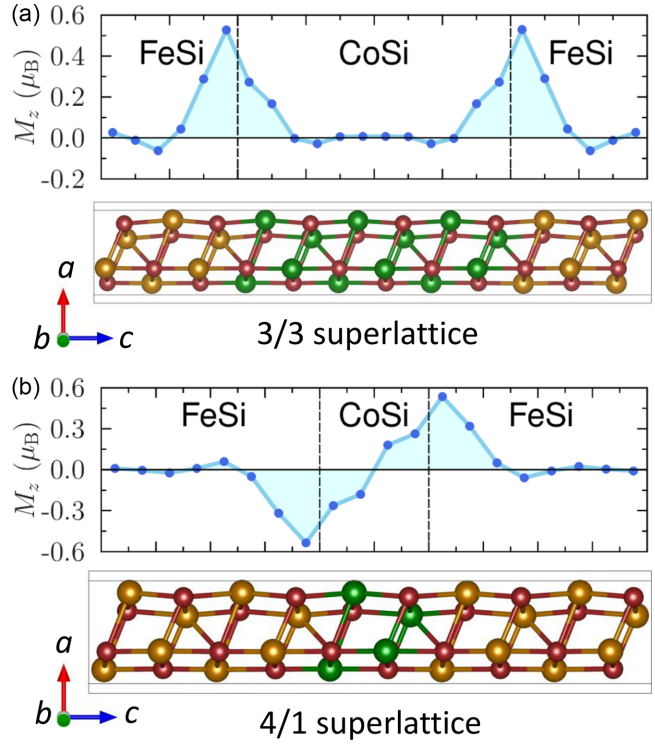

FIG. 2. Layer-resolved magnetic moments on the Fe and Co sites in the (a) $(FeSi)_3/(CoSi)_3$ and (b) $(FeSi)_4/(CoSi)_1$ superlattices; the interfaces are marked by vertical dashed lines. Below each plot, a structural sketch of the system is shown, where Fe (light brown) and Co (green) sites are connected by Si (red brown).

magnetic but the two interfaces are antiferromagnetically coupled, so the resulting magnetization of the system is zero [Fig. 2(b)]. The AFM ordering in the 4/1 superlattice, however, indicates significantly different magnetic interactions compared to the 3/3 system.

We note that the emergence of magnetism at the interfaces which we find in the studied B20 multilayers is predicted both by GGA and by LSDA approximations of density functional theory, as discussed in Sec. VII of the SM [32], which supports the conclusions of our theoretical study.

The simulated annealing procedure, where one goes from high to low temperatures in the ASD simulations, allows to predict the magnetic state of the $(FeSi)_3/(CoSi)_3$ system at zero external field, which is a spin spiral with a period around 45 nm, as shown in Fig. 3(a). When a finite magnetic field is applied to the system perpendicular to the interfaces (z direction), the spirals start to split [Figs. S1(b) and S1(c)] and around 300 mT one sees the formation of multiple isolated, elongated along the [110] direction, antiskyrmions with a size ~14 nm [Fig. 3(b)] as well as one intermediate skyrmion with a size ~8 nm [Fig. S3(a)]. The 2/2 superlattice shows a very similar behavior [Figs. S1(e)–S1(h)]. Usually, skyrmions have a helicity of either 0 (Néel skyrmion) or $\pi/2$ (Bloch skyrmion). For the intermediate skyrmion, the helicity deviates from these two limits, but is closer to the Bloch limit for the $(FeSi)_3/(CoSi)_3$ multilayer, as can be seen from a close-up of this texture [Fig. S3(a)]. Using the methodology discussed in Ref. [51], we calculate the topological charge −1 for the

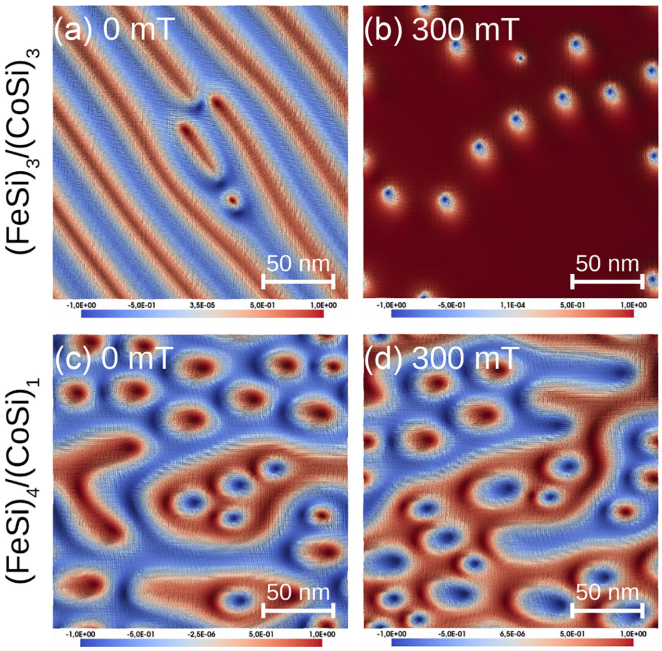

FIG. 3. Predicted magnetic state of the (a), (b) $(FeSi)_3/(CoSi)_3$ and (c), (d) $(FeSi)_4/(CoSi)_1$ superlattices at zero and finite external magnetic field perpendicular to the interfaces from atomistic spin dynamics simulations of annealing from 300 K to zero temperature. The size of the simulated region is around (220×220) nm^2 and includes 10^6 spins for (a) and (b) and 2×10^6 spins for (c) and (d). The color code depicts the z component of spin, which varies between -1 and $+1$.

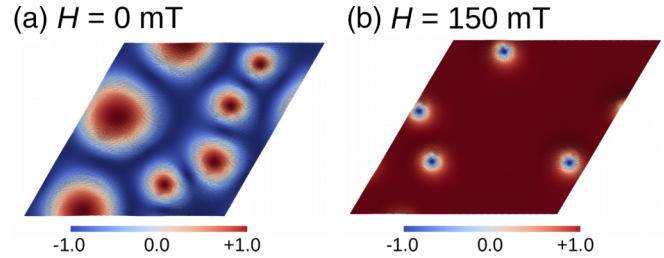

FIG. 4. Predicted magnetic state of the [111]-oriented $(FeSi)_3/(CoSi)_3$ superlattice at (a) zero and (b) finite external magnetic field $H = 150$ mT along the [111] direction from atomistic spin dynamics simulations of annealing from 300 K to zero temperature. The simulated region has a side length of around 157 nm and 60° angle in between and includes 8.75×10^5 spins. In both plots, the pointlike topological objects are intermediate skyrmions. The color code depicts the z component of spin, which varies between -1 and $+1$.

observed antiskyrmions and $+1$ for the intermediate skyrmions. At higher fields around 400–500 mT the antiskyrmions become smaller and less distorted [~7–8 nm in Fig. 1(c)] and, finally, above 600 mT the system becomes fully ferromagnetic (FM phase). Monte Carlo simulations for the FM state in zero field allow to estimate the critical temperature T_C for magnetic ordering to be around 40 K [Fig. S4(a)]. It may seem lower than T_C of bulk $Fe_{0.5}Co_{0.5}Si$ seen in Fig. S4(e), but the latter is overestimated by theory compared to the measured values around 30 K. Based on this, we expect that the thermal stability of the [001]-FeSi/CoSi superlattice is similar to the bulk counterpart.

In contrast, for the $(FeSi)_4/(CoSi)_1$ superlattice we find antiferromagnetically (AFM) coupled interfaces with zero net magnetization, as mentioned already above and shown in Fig. 2(b). However, the distribution of magnetization near each interface contains interesting features, shown in Figs. 3(c) and 3(d) for one of the interfaces (the other interface nearby has opposite magnetization but the same distribution in real space). At zero field, we find a number of distorted antiskyrmions ~18–37 nm with topological charge -1 embedded in locally ferromagnetic (FM) domains and their number changes in an applied magnetic field, but their average size is barely affected and the total magnetization of each interface is around or below $0.15\,\mu_B$ per $(500 \times 500 \times 1)$ supercell, meaning that it is magnetically almost compensated. In a way, this FeSi/CoSi system represents a synthetic antiferromagnet with topological magnetic textures. Due to the strong AFM coupling between the interfaces, the system is not easy to polarize even by external magnetic field up to 1 T [see Fig. 3(d) and Figs. S2(b)–S2(d)], nor is it easy to manipulate the antiskyrmions, compared to the 3/3 and 2/2 superlattices. This unusual resilience to perturbations from a magnetic field may offer unique advantages for applications. Based on the temperature-dependent simulations of the collinear AFM phase [Fig. S4(c)], we expect that antiskyrmions in the 4/1 superlattice can be stable below 90 K. Note that magnetic anisotropy effects in this system can be important, as our calculations show (see details in Sec. VIII of the SM [32]).

We also considered the [111]-oriented $(FeSi)_3/(CoSi)_3$ multilayer where, similarly to the [001] interfaces, magnetism emerges at the interfaces, while the interfaces are separated by almost nonmagnetic regions. From the ASD simulations using a $(250 \times 250 \times 1)$ supercell with 875 000 atomic moments we find the zero-field magnetic state containing intermediate skyrmions with topological charge $+1$ [Fig. 4(a)], which is in contrast to the zero-field spin-spiral phase of the [001] interface. In an external magnetic field between 100 and 200 mT, these skyrmions become more compact [Fig. 4(b)]; their diameter varies monotonically between 24 nm at $H = 100$ mT and 12 nm at $H = 200$ mT. At fields above 300 mT, the system becomes fully ferromagnetic, and the critical temperature of the FM phase in zero field from Monte Carlo simulations is similar to the [001]-oriented superlattice [Fig. S4(a)].

For comparison, we consider also the $(FeSi)_m/(FeGe)_n$ superlattices (all figures are in the SM [32]). The main difference between the FeSi/FeGe and FeSi/CoSi systems is that FeGe already shows finite magnetic moments in the bulk, while CoSi does not. Near the [001]-oriented interface, however, we find that the FeGe magnetization is reduced considerably compared to the bulk material (Fig. S5), which decreases the critical temperature for the 3/1 superlattice compared to bulk, while the 3/3 superlattice is more reminiscent of bulk [compare Figs. S4(b), S4(d), and S4(f)]. Also, nonzero moments $\sim 0.3\,\mu_B$ are induced in the neighboring FeSi layer; these are, however, not included in our spin model due to their much smaller magnitude compared to the Fe moments in FeGe. For the [111]-oriented $(FeSi)_3/(FeGe)_1$ multilayer, we could

not stabilize any sizable moments on Fe sites in the RSPT calculations.

The ASD annealing simulations for the $(FeSi)_3/(FeGe)_1$ superlattice using a $(500 \times 500 \times 1)$ supercell containing 10^6 spins predict a spin spiral phase at zero field with a comparably large spatial period of around 100 nm [Fig. S2(e)]. Interestingly, this system appears to be more sensitive to external magnetic field than the other systems that we studied, since already for $H = 40$ mT it becomes fully ferromagnetic. At a slightly smaller field $H = 30$ mT we see isolated Bloch skyrmions with topological charge $+1$ [Figs. S2(h) and S3(d)], which are also known for bulk FeGe in a similar range of fields [schematic view in Fig. 1(a)]. In our multilayer, however, the skyrmions are much more compact ($\sim$8 nm) than in bulk FeGe where the characteristic magnetic length scale is 70 nm [27,52,53]. These results hold irrespective of whether the induced Fe moments in FeSi are included or excluded from the spin model (see Sec. IX in the SM [32]).

To analyze the origin of the magnetic topological textures observed in our simulations, we calculate and compare the micromagnetic parameters of the studied multilayers, which is easier than analyzing the corresponding atomistic interactions for hundreds of atomic neighbors. We do not perform actual micromagnetic simulations in this work, because the atomistic spin dynamics is a more accurate and straightforward way to simulate these systems with several magnetic atoms per unit cell and quite small skyrmions of the order of several nanometers. Nevertheless, we make a note on how to calculate the micromagnetic parameters and effective field in Secs. IV and VI of the SM [32].

The micromagnetic quantities A and $\langle D \rangle = \sum D_{\alpha\beta}$ for the different B20 superlattices are collected in Table I in the SM [32] and give an overall impression of the strength of Heisenberg and Dzyaloshinskii-Moriya interactions. First, we notice that the 4/1 superlattice appears to show a somewhat smaller $A/\langle D \rangle$ ratio (i.e., more pronounced DM interaction) compared to the 3/3 superlattice. We argue that this is related to the smaller distance between the interfaces in the 4/1 system, which probably enhances their symmetry breaking effect. Importantly, for bulk $Fe_{0.5}Co_{0.5}Si$ (see Table I in the SM [32]) we find weaker bulk-type DMI and $A/\langle D \rangle$ ratio which is almost an order of magnitude larger than the corresponding values for the FeSi/CoSi superlattices, suggesting that nanoscale B20 multilayers can be, indeed, more promising in terms of topological magnetism. For FeSi/FeGe, the increase of DMI compared to bulk is less pronounced, but the structure of the DM matrix is changed and we find rather small Bloch skyrmions in a narrow field range. The important finding of our work is that the B20 multilayers show a more complicated DM matrix compared to the diagonal $D_{\alpha\beta}$ of bulk B20 compounds (see Table I in the SM [32]) or simple D_{xy}-type matrix of transition metal multilayers, leading to stabilization of spin textures beyond Néel or Bloch skyrmions (Fig. 1).

In conclusion, the B20 multilayers, studied here using state-of-the-art first-principles methods, show a potential for interesting topological magnetism, that can be different both from that of the bulk B20 compounds and many other metallic multilayers. While our theoretical predictions may be quantitatively off in terms of value of magnetic moments induced at the interfaces and Curie temperature, we believe that the theoretical results provide strong indications of a large variety of topological magnetic characters of the proposed B20 multilayers. The interface orientation and layer thicknesses appear to change the character of the magnetism as well as the topological textures, which include antiskyrmions and intermediate skyrmions coexisting near FeSi/CoSi interfaces and Bloch skyrmions in FeSi/FeGe multilayer, all in the range of sizes $\sim$(7–37) nm. Further opportunities for tuning the DMI in these multilayers systems could be, for example, chemical doping, which is known to be effective for bulk B20 compounds (see, e.g., Ref. [54]). For most systems that we propose here, it is not necessary to have atomically thin B20 layers; instead, a single interface between two B20 films can host skyrmions too, as our results suggest. For technological applications we highlight the $(FeSi)_4/(CoSi)_1$ system due to its stability in magnetic field and the AFM skyrmions that should have zero skyrmion Hall effect [55]. Our theoretical predictions call for experimental verifications and motivate studies of similar systems where both magnetism and chiral interactions are induced by nanoscale interfaces.

Acknowledgments. This work was financially supported by the Knut and Alice Wallenberg Foundation through Grants No. 2018.0060, No. 2021.0246, and No. 2022.0108, and Göran Gustafsson Foundation (recipient of the "small prize": V.B.). O.E. and A.D. acknowledge support from the Wallenberg Initiative Materials Science for Sustainability (WISE) funded by the Knut and Alice Wallenberg Foundation (KAW). A.D. also acknowledges financial support from the Swedish Research Council (Vetenskapsrådet, VR), Grants No. 2016-05980 and No. 2019-05304. O.E. also acknowledges support by the Swedish Research Council (VR), the Foundation for Strategic Research (SSF), the Swedish Energy Agency (Energimyndigheten), the European Research Council (854843-FASTCORR), eSSENCE, and STandUP. The computations/data handling were enabled by resources provided by the Swedish National Infrastructure for Computing (SNIC) at the National Supercomputing Centre (NSC, Tetralith cluster) partially funded by the Swedish Research Council through Grant Agreement No. 2018-05973 and by the National Academic Infrastructure for Supercomputing in Sweden (NAISS) at the National Supercomputing Centre (NSC, Tetralith cluster) partially funded by the Swedish Research Council through Grant Agreement No. 2022-06725. Figures 1(a) and 1(b) were produced by the PARAVIEW software [56] and structural sketches in Fig. 2 by the VESTA3 software [57].

[1] R. Wood, The feasibility of magnetic recording at 1 Terabit per square inch, IEEE Trans. Magn. **36**, 36 (2000).

[2] A. Fert, V. Cros, and J. Sampaio, Skyrmions on the track, Nat. Nanotechnol. **8**, 152 (2013).

[3] J. Jena, B. Göbel, T. Ma, V. Kumar, R. Saha, I. Mertig, C. Felser, and S. S. P. Parkin, Elliptical Bloch skyrmion chiral twins in an antiskyrmion system, Nat. Commun. **11**, 1115 (2020).

[4] Y. Huang, W. Kang, X. Zhang, Y. Zhou, and W. Zhao, Magnetic skyrmion-based synaptic devices, Nanotechnology **28**, 08LT02 (2017).

[5] G. Bourianoff, D. Pinna, M. Sitte, and K. Everschor-Sitte, Potential implementation of reservoir computing models based on magnetic skyrmions, AIP Adv. **8**, 055602 (2018).

[6] D. Pinna, F. Abreu Araujo, J.-V. Kim, V. Cros, D. Querlioz, P. Bessiere, J. Droulez, and J. Grollier, Skyrmion gas manipulation for probabilistic computing, Phys. Rev. Appl. **9**, 064018 (2018).

[7] B. Göbel, I. Mertig, and O. A. Tretiakov, Beyond skyrmions: Review and perspectives of alternative magnetic quasiparticles, Phys. Rep. **895**, 1 (2021).

[8] S. Mühlbauer, B. Binz, F. Jonietz, C. Pfleiderer, A. Rosch, A. Neubauer, R. Georgii, and P. Böni, Skyrmion lattice in a chiral magnet, Science **323**, 915 (2009).

[9] I. Kézsmárki, S. Bordács, P. Milde, E. Neuber, L. M. Eng, J. S. White, H. M. Rønnow, C. D. Dewhurst, M. Mochizuki, K. Yanai, H. Nakamura, D. Ehlers, V. Tsurkan, and A. Loidl, Néel-type skyrmion lattice with confined orientation in the polar magnetic semiconductor GaV_4S_8, Nat. Mater. **14**, 1116 (2015).

[10] N. Kanazawa, S. Seki, and Y. Tokura, Noncentrosymmetric magnets hosting magnetic skyrmions, Adv. Mater. **29**, 1603227 (2017).

[11] A. Soumyanarayanan, M. Raju, A. L. G. Oyarce, A. K. C. Tan, M.-Y. Im, A. P. Petrović, P. Ho, K. H. Khoo, M. Tran, C. K. Gan, F. Ernult, and C. Panagopoulos, Tunable room-temperature magnetic skyrmions in Ir/Fe/Co/Pt multilayers, Nat. Mater. **16**, 898 (2017).

[12] S. Heinze, K. von Bergmann, M. Menzel, J. Brede, A. Kubetzka, R. Wiesendanger, G. Bihlmayer, and S. Blügel, Spontaneous atomic-scale magnetic skyrmion lattice in two dimensions, Nat. Phys. **7**, 713 (2011).

[13] N. Romming, C. Hanneken, M. Menzel, J. E. Bickel, B. Wolter, K. von Bergmann, A. Kubetzka, and R. Wiesendanger, Writing and deleting single magnetic skyrmions, Science **341**, 636 (2013).

[14] A. N. Bogdanov and U. K. Rößler, Chiral symmetry breaking in magnetic thin films and multilayers, Phys. Rev. Lett. **87**, 037203 (2001).

[15] X. Li, W. V. Liu, and L. Balents, Spirals and skyrmions in two dimensional oxide heterostructures, Phys. Rev. Lett. **112**, 067202 (2014).

[16] A. K. Nandy, N. S. Kiselev, and S. Blügel, Interlayer exchange coupling: A general scheme turning chiral magnets into magnetic multilayers carrying atomic-scale skyrmions, Phys. Rev. Lett. **116**, 177202 (2016).

[17] W. H. Butler, X.-G. Zhang, T. C. Schulthess, and J. M. MacLaren, Spin-dependent tunneling conductance of Fe|MgO|Fe sandwiches, Phys. Rev. B **63**, 054416 (2001).

[18] M. Bowen, V. Cros, F. Petroff, A. Fert, C. Martinez Boubeta, J. L. Costa-Kråmer, J. V. Anguita, A. Cebollada, F. Briones, J. M. de Teresa, L. Morellón, M. R. Ibarra, F. Güell, F. Peiró, and A. Cornet, Large magnetoresistance in Fe/MgO/FeCo(001) epitaxial tunnel junctions on GaAs(001), Appl. Phys. Lett. **79**, 1655 (2001).

[19] O. Jepsen, J. Madsen, and O. Andersen, Spin density in thin Ni (100)-films by the self-consistent LAPW method, J. Magn. Magn. Mater. **15-18**, 867 (1980).

[20] O. Eriksson, G. Fernando, R. Albers, and A. Boring, Enhanced orbital contribution to surface magnetism in Fe, Co, and Ni, Solid State Commun. **78**, 801 (1991).

[21] J. T. Lau, A. Föhlisch, M. Martins, R. Nietubyc, M. Reif, and W. Wurth, Spin and orbital magnetic moments of deposited small iron clusters studied by x-ray magnetic circular dichroism spectroscopy, New J. Phys. **4**, 98 (2002).

[22] M. Tischer, O. Hjortstam, D. Arvanitis, J. H. Dunn, F. May, K. Baberschke, J. Trygg, J. M. Wills, B. Johansson, and O. Eriksson, Enhancement of orbital magnetism at surfaces: Co on Cu(100), Phys. Rev. Lett. **75**, 1602 (1995).

[23] C. Pfleiderer, M. Uhlarz, S. M. Hayden, R. Vollmer, H. v. Löhneysen, N. R. Bernhoeft, and G. G. Lonzarich, Coexistence of superconductivity and ferromagnetism in the *d*-band metal $ZrZn_2$, Nature (London) **412**, 58 (2001).

[24] G. Aeppli and Z. Fisk, Kondo insulators, Comments Condens. Matter Phys. **16**, 155 (1992).

[25] J. H. Wernick, G. K. Wertheim, and R. C. Sherwood, Magnetic behavior of the monosilicides of the 3*d*-transition elements, Mater. Res. Bull. **7**, 1431 (1972).

[26] X. Z. Yu, Y. Onose, N. Kanazawa, J. H. Park, J. H. Han, Y. Matsui, N. Nagaosa, and Y. Tokura, Real-space observation of a two-dimensional skyrmion crystal, Nature (London) **465**, 901 (2010).

[27] X. Z. Yu, N. Kanazawa, Y. Onose, K. Kimoto, W. Z. Zhang, S. Ishiwata, Y. Matsui, and Y. Tokura, Near room-temperature formation of a skyrmion crystal in thin-films of the helimagnet FeGe, Nat. Mater. **10**, 106 (2011).

[28] V. Borisov, Q. Xu, N. Ntallis, R. Clulow, V. Shtender, J. Cedervall, M. Sahlberg, K. T. Wikfeldt, D. Thonig, M. Pereiro, A. Bergman, A. Delin, and O. Eriksson, Tuning skyrmions in B20 compounds by 4*d* and 5*d* doping, Phys. Rev. Mater. **6**, 084401 (2022).

[29] V. Borisov, N. Salehi, M. Pereiro, A. Delin, and O. Eriksson, Dzyaloshinskii-Moriya interactions, Néel skyrmions and V_4 magnetic clusters in multiferroic lacunar spinel GaV_4S_8, npj Comput. Mater. **10**, 53 (2024).

[30] P. Hohenberg and W. Kohn, Inhomogeneous electron gas, Phys. Rev. **136**, B864 (1964).

[31] J. P. Perdew, K. Burke, and M. Ernzerhof, Generalized gradient approximation made simple, Phys. Rev. Lett. **77**, 3865 (1996).

[32] See Supplemental Material at http://link.aps.org/supplemental/10.1103/PhysRevB.110.L060407 for further information and discussion of the magnetic properties obtained from first-principles calculations and spin-dynamics simulations.

[33] M. Poluektov, O. Eriksson, and G. Kreiss, Coupling atomistic and continuum modelling of magnetism, Comput. Methods Appl. Mech. Eng. **329**, 219 (2018).

[34] R. D. Collyer and D. A. Browne, Correlations and the magnetic moment of MnSi, Phys. B: Condens. Matter **403**, 1420 (2008).

[35] S. Grytsiuk, M. Hoffmann, J.-P. Hanke, P. Mavropoulos, Y. Mokrousov, G. Bihlmayer, and S. Blügel, *Ab initio* analysis of magnetic properties of the prototype B20 chiral magnet FeGe, Phys. Rev. B **100**, 214406 (2019).

[36] M. Pajda, J. Kudrnovský, I. Turek, V. Drchal, and P. Bruno, *Ab initio* calculations of exchange interactions, spin-wave stiffness constants, and Curie temperatures of Fe, Co, and Ni, Phys. Rev. B **64**, 174402 (2001).

[37] Y. Onose, N. Takeshita, C. Terakura, H. Takagi, and Y. Tokura, Doping dependence of transport properties in $Fe_{1-x}Co_xSi$, Phys. Rev. B **72**, 224431 (2005).

[38] C. S. Spencer, J. Gayles, N. A. Porter, S. Sugimoto, Z. Aslam, C. J. Kinane, T. R. Charlton, F. Freimuth, S. Chadov, S. Langridge, J. Sinova, C. Felser, S. Blügel, Y. Mokrousov, and C. H. Marrows, Helical magnetic structure and the anomalous and topological Hall effects in epitaxial B20 $Fe_{1-y}Co_yGe$ films, Phys. Rev. B **97**, 214406 (2018).

[39] J. M. Wills and B. R. Cooper, Synthesis of band and model Hamiltonian theory for hybridizing cerium systems, Phys. Rev. B **36**, 3809 (1987).

[40] J. M. Wills, O. Eriksson, P. Andersson, A. Delin, O. Grechnyev, and M. Alouani, Full-potential electronic structure method, in *Energy and Force Calculations with Density Functional and Dynamical Mean Field Theory*, Springer Series in Solid-State Science Vol. 167 (Springer, Berlin, Heidelberg, 2010).

[41] J. M. Wills, O. Eriksson, M. Alouani, and D. L. Price, Full-potential LMTO total energy and force calculations, in *Electronic Structure and Physical Properties of Solids*, edited by H. Dreyssé (Springer-Verlag, Berlin, Heidelberg, 2000), pp. 148–167.

[42] S. Bahn and K. Jacobsen, An object-oriented scripting interface to a legacy electronic structure code, Comput. Sci. Eng. **4**, 56 (2002).

[43] A. H. Larsen, J. J. Mortensen, J. Blomqvist, I. E. Castelli, R. Christensen, M. Dułak, J. Friis, M. N. Groves, B. Hammer, C. Hargus, E. D. Hermes, P. C. Jennings, P. B. Jensen, J. Kermode, J. R. Kitchin, E. L. Kolsbjerg, J. Kubal, K. Kaasbjerg, S. Lysgaard, J. B. Maronsson *et al.*, The atomic simulation environment—a Python library for working with atoms, J. Phys.: Condens. Matter **29**, 273002 (2017).

[44] G. Kresse and J. Furthmüller, Efficient iterative schemes for *ab initio* total-energy calculations using a plane-wave basis set, Phys. Rev. B **54**, 11169 (1996).

[45] A. I. Liechtenstein, M. I. Katsnelson, V. P. Antropov, and V. A. Gubanov, Local spin density functional approach to the theory of exchange interactions in ferromagnetic metals and alloys, J. Magn. Magn. Mater. **67**, 65 (1987).

[46] A. Szilva, Y. Kvashnin, E. A. Stepanov, L. Nordström, O. Eriksson, A. I. Lichtenstein, and M. I. Katsnelson, Quantitative theory of magnetic interactions in solids, Rev. Mod. Phys. **95**, 035004 (2023).

[47] B. Skubic, J. Hellsvik, L. Nordström, and O. Eriksson, A method for atomistic spin dynamics simulations: Implementation and examples, J. Phys.: Condens. Matter **20**, 315203 (2008).

[48] O. Eriksson, A. Bergman, L. Bergqvist, and J. Hellsvik, Atomistic Spin Dynamics: Foundations and Applications, *Atomistic Spin Dynamics: Foundations and Applications* (Oxford University Press, Oxford, UK, 2017).

[49] L. Landau and E. Lifshitz, On the theory of the dispersion of magnetic permeability in ferromagnetic bodies, in *Perspectives in Theoretical Physics* (Pergamon, Amsterdam, 1992), pp. 51–65. Reprinted from Phys. Z. Sowjetunion **8**, Part 2, 153, (1935).

[50] T. Gilbert, A phenomenological theory of damping in ferromagnetic materials, IEEE Trans. Magn. **40**, 3443 (2004).

[51] J.-V. Kim and J. Mulkers, On quantifying the topological charge in micromagnetics using a lattice-based approach, IOP SciNotes **1**, 025211 (2020).

[52] B. Lebech, J. Bernhard, and T. Freltoft, Magnetic structures of cubic FeGe studied by small-angle neutron scattering, J. Phys.: Condens. Matter **1**, 6105 (1989).

[53] M. Uchida, N. Nagaosa, J. P. He, Y. Kaneko, S. Iguchi, Y. Matsui, and Y. Tokura, Topological spin textures in the helimagnet FeGe, Phys. Rev. B **77**, 184402 (2008).

[54] Y. Guang, Y. Fujishiro, A. Tanaka, L. Peng, Y. Kaneko, N. Kanazawa, Y. Tokura, and X. Yu, Topological stability of spin textures in Si/Co-doped helimagnet FeGe, J. Phys. Mater. **7**, 025009 (2024).

[55] X. Zhang, Y. Zhou, and M. Ezawa, Magnetic bilayer-skyrmions without skyrmion Hall effect, Nat. Commun. **7**, 10293 (2016).

[56] ParaView – Open-source, multi-platform data analysis and visualization application, https://www.paraview.org/.

[57] K. Momma and F. Izumi, Vesta 3 for three-dimensional visualization of crystal, volumetric and morphology data, J. Appl. Crystallogr. **44**, 1272 (2011).